IMPROVED YIELD DETERMINATION AND EVENT IDENTIFICATION RESEARCH

J. M. Savino, et al

Systems, Science and Software

Prepared for:

Air Force Technical Applications Center

17 November 1975

089060

SYSTEMS, SCIENCE AND SOFTWARE

SSS-R-76-2788

IMPROVED YIELD DETERMINATION AND EVENT IDENTIFICATION RESEARCH

J. M. Savino
T. C. Bache
T. G. Barker
J. T. Cherry
W. O. Wray

Quarterly Technical Report
For Period August 1, 1975 - October 31, 1975

Sponsored by:

Advanced Research Projects Agency
ARPA Order No. 2551

This research was supported by the Advanced Research Projects Agency of the Department of Defense and was monitored by AFTAC/VSC, Patrick AFB, FL 32925, under Contract No. F08606-75-C-0045.

S^3 Project No. 11014

November 17, 1975

P. O. BOX 1620, LA JOLLA, CALIFORNIA 92038. TELEPHONE (714) 453-0060

UNCLASSIFIED

SECURITY CLASSIFICATION OF THIS PAGE (When Data Entered)

REPORT DOCUMENTATION PAGE		READ INSTRUCTIONS BEFORE COMPLETING FORM
1. REPORT NUMBER	2. GOVT ACCESSION NO.	3. RECIPIENT'S CATALOG NUMBER
4. TITLE (and Subtitle) Improved Yield Determination and Event Identification Research		5. TYPE OF REPORT & PERIOD COVERED Quarterly Technical Report Aug. 1, 1975 - Oct. 31, 1975
		6. PERFORMING ORG. REPORT NUMBER SSS-R-76-2788
7. AUTHOR(s) J. M. Savino, T. C. Bache, T. G. Barker J. T. Cherry and W. O. Wray		8. CONTRACT OR GRANT NUMBER(s) Contract No. F08606-75-C-0045
9. PERFORMING ORGANIZATION NAME AND ADDRESS Systems, Science and Software P. O. Box 1620 La Jolla, CA 92038		10. PROGRAM ELEMENT, PROJECT, TASK AREA & WORK UNIT NUMBERS Program Code No. 6F10 ARPA Order No. 2551
11. CONTROLLING OFFICE NAME AND ADDRESS VELA Seismological Center 312 Montgomery Street Alexandria, VA 22314		12. REPORT DATE November 17, 1975 13. NUMBER OF PAGES 48
14. MONITORING AGENCY NAME & ADDRESS(if different from Controlling Office)		15. SECURITY CLASS. (of this report) Unclassified 15a. DECLASSIFICATION/DOWNGRADING SCHEDULE

16. DISTRIBUTION STATEMENT (of this Report)

Approved for Public Release, Distribution Unlimited

17. DISTRIBUTION STATEMENT (of the abstract entered in Block 20, if different from Report)

18. SUPPLEMENTARY NOTES

19. KEY WORDS (Continue on reverse side if necessary and identify by block number)
Magnitude-yield relationships, Yield determination, Seismic coupling, Earth structure, Ground motion prediction, Explosive source modeling, Multiple explosion modeling.

20. ABSTRACT (Continue on reverse side if necessary and identify by block number)

Teleseismic ground motion predictions for the recent Pahute Mesa explosion, MAST, were quite successful in terms of both amplitude and waveform matching. The predicted short-period body wave amplitudes were within 30 to 50 percent of the observed amplitudes at most of the SDCS stations. In addition, the general character of the first few seconds of the P-wave trains at the various SDCS stations were matched in reasonable detail.

(over)

DD FORM 1 JAN 73 1473 EDITION OF 1 NOV 65 IS OBSOLETE

UNCLASSIFIED

SECURITY CLASSIFICATION OF THIS PAGE (When Data Entered)

A tension failure model that describes the development of a region of enhanced tension failure (cracking) produced during stress release behind the interacting shock fronts from closely spaced explosions was developed. Calculations for a multiple explosion scenario (three closely spaced explosions detonated simultaneously) were carried out into the elastic region using the two-dimensional CRAM code with the new material failure model included.

AFTAC Project Authorization No. VELA T/6712/B/ETR

Program Code No. 6F10

Effective Date of Contract: May 1, 1975

Contract No. F08606-75-C-0045

Principal Investigator and Phone No.
Dr. John M. Savino (714) 453-0060, Ext. 455

Project Scientist and Phone No.
Dr. Ralph W. Alewine, III (703) 325-8484

TABLE OF CONTENTS

		Page
LIST OF ILLUSTRATIONS		2
I.	SUMMARY	3
II.	INTRODUCTION	6
III.	TECHNICAL DISCUSSION	7
3.1	GROUND MOTION PREDICTIONS FOR THE MAST EVENT	7
3.1.1	Body Waves	7
3.1.2	Rayleigh Waves	20
3.2	MULTIPLE BURST CALCULATION	25
3.2.1	Introduction	25
3.2.2	Discussion of the Tension Failure Model	25
3.2.3	Results of Multiple Burst Calculation	32
3.2.4	Summary	32
3.3	SEISMIC COUPLING FROM A NUCLEAR EXPLOSION	37
3.3.1	Dependence of Seismic Coupling on the Near Explosion Source Environment.	37
3.3.2	Constitutive Modeling	39
IV.	CONCLUSIONS	40
V.	REFERENCES	41

LIST OF ILLUSTRATIONS

Figure		Page
3.1	Comparison of theoretical (left) and observed seismograms for Mast at five SDCS stations . .	11
3.2	Comparison of theoretical and observed seismograms as in Fig. 3.1 except that the upper mantle model HWNE was used	12
3.3	Comparison of observed and theoretical "b" amplitudes from Figs. 3.1 and 3.2	13
3.4	Comparison of observed and theoretical "d" amplitudes from Figs. 3.1 and 3.2	14
3.5	Short period vertical seismograms: observations on the right, and synthetics for the model HWA-2 on the left	16
3.6	Short period vertical seismograms: observations on the right and synthetics for model HWNE-3 on the left	17
3.7	Comparison of observed and theoretical "b" amplitudes from the records of Figs. 3.5 and 3.6	18
3.8	Comparison of predicted and observed "d" amplitudes from the records of Figs. 3.5 and 3.6	19
3.9	The theoretical long period record for HNME and the comparison of theoretical and observed long period data at RKON, CPSO, WHY2K and FNWV	21
3.10	Comparison of predicted and observed Airy phase amplitudes from the records of Fig. 3.9 . . .	24
3.11	Schematic definition of the crack angle α and the failure coordinates	28
3.12	Relative orientation of the principal and failure coordinate systems	29
3.13	Crack location and orientation 4.93 msec after detonation	33
3.14	Crack location and orientation 6.85 msec after detonation	34
3.15	Crack location and orientation 9.21 msec after detonation	35
3.16	Crack location and orientation 11.5 msec after detonation	36

I. SUMMARY

During the past several years, Systems, Science and Software (S^3) personnel have been actively engaged in a comprehensive program involving computer modeling of the nonlinear processes that characterize underground nuclear explosions, propagation of the resultant stress waves through realistic earth structures and prediction of the ground motion recorded at teleseismic distances from an explosion. The objectives of the subject project are to employ these modeling and predictive capabilities in a systematic examination of the effects of variations in source and emplacement parameters on seismic signals from underground explosions, and to investigate methods for utilizing the general characteristics of seismic waveforms to obtain reliable yield estimates for explosions.

The technical phases necessary to accomplish the objectives of this project are as follows:

1. Conduct a systematic theoretical examination of material, source and emplacement parameters which affect yield-magnitude relationships and compare the theoretical predictions to actual observations.

2. Determine and express uncertainties of yield estimates in terms of uncertainties in gross earth structure, near source material properties, and local source and receiver structure.

Major accomplishments during the second three-month period of this project were realized in several different areas of research. Of particular importance was the exercise of our computational capabilities for the prediction of teleseismically recorded body and surface waves from the recent Pahute Mesa explosion, MAST. Our objective in

this experiment was to model the near source (explosion) nonlinear processes, propagate the resultant stress waves through realistic earth structures and finally, generate synthetic seismograms for comparison with actual recordings obtained from five Special Data Collection Stations (SDCS) located at teleseismic distances from the Nevada Test Site (NTS).

Our ground motion predictions for MAST were quite successful in terms of both amplitude and waveform matching. For instance, the predicted short-period body wave amplitudes were within 30-50 percent of the observed amplitudes at most of the SDCS stations. In addition, the character of the first few seconds of the P-wave train at the various SDCS station were matched in some detail. A technical report (Bache, et al., 1975a) describing the initial ground motion predictions for MAST was submitted during this contractual report period. A more detailed report that describes the iterative procedure adopted for the final ground motion computations is in preparation and will be submitted shortly.

Another major area of on-going investigation is the computation of the seismic coupling resulting from the simultaneous detonation of three closely spaced nuclear sources. Our efforts during this past quarter focussed on the development of a tension failure model that describes the development of a region of enhanced tension failure (cracking) produced during stress release behind the interacting shock fronts. This region is a unique feature of the nonlinear material behavior produced by the simultaneous detonation of closely spaced explosives. The multiple burst calculation has been carried out into the elastic region using the two dimensional CRAM code with the new material failure model included.

A technical report (Cherry, et al., 1975a) that describes the results of an explosion near source material parameter study was prepared and submitted during this reporting period. The objective of the research presented in this report was to determine the dependence of teleseismic magnitudes on the nonlinear behavior of the near explosion source rock environment. Such information enables one to express uncertainties in explosive yield estimates in terms of uncertainties in the material properties and provides insight concerning the requirements for collection of geophysical data at a specific test site. The conduct of the Limited Yield Test Ban Treaty should be greatly facilitated by the availability of this information.

II. INTRODUCTION

As stated in the previous section, the objectives of the subject research project are to utilize existing computational capabilities to examine the effects of various source and emplacement parameters on seismic signals from underground explosions, and to devise and evaluate methods for utilizing the general characteristics of seismic waveforms to obtain reliable estimates of explosion yields. In order to realize these objectives, activity on this program during the second three-month period of this contract concentrated in the following areas:

1. The prediction of teleseismic ground motion, body and surface waves, generated by specific NTS explosions and recorded at selected seismograph stations.
2. Modeling of the source region of a multiple underground nuclear explosion scenario and computation of the seismic coupling from such an event.
3. Investigation of the dependence of the seismic coupling of a nuclear explosion on the nonlinear behavior of the near explosion source rock environment.

The plan of the remainder of this report is to present technical discussions of each of these three research areas, followed by a section summarizing the most important results obtained to date.

III. TECHNICAL DISCUSSION

3.1 GROUND MOTION PREDICTIONS FOR THE MAST EVENT

It was requested that S^3 predict the short and long period seismograms recorded for the Mast event at five specified SDCS stations. An initial prediction was made using the best available information for the rock properties at the working point and the near source geology. Standard earth models were used for the propagation path. Upon comparing our predictions to the actual data, we concluded that much, if not most, of the observed discrepancy was due to propagation path effects. Improved modeling of the propagation path is expected to lead to improved predictions of future events.

In this section we first summarize our initial predictions of Mast and the comparison with data. After studying the comparison we made adjustments to our models of the propagation path and the improved results are also summarized.

3.1.1 Body Waves

The computational method for the prediction of body waves employs the following:

1. The reduced displacement potential (RDP) is computed by our spherically symmetric, one-dimensional finite difference code (SKIPPER).
2. The RDP is input to a code which computes the detailed crustal reverberations for an equivalent elastic source buried in a stack of plane elastic layers (see Appendix B, Bache, et al. (1975b) for the theory).
3. Detailed crustal reverberations at the receiver are computed using the method of Haskell (1962).

4. Travel through the upper mantle is computed by generalized ray theory as implemented by Helmberger and described in Wiggins and Helmberger (1974).

5. The desired sensing instrument transfer function is applied to the ground motion.

For surface waves, steps 2-4 are replaced by:

2. The Rayleigh wave dispersion data and amplitude excitation for a plane layered earth model is computed using the method of Harkrider (1964, 1970).

3. The source time history is convolved with the earth response function.

The pertinent data were obtained from the following sources:

1. The material properties of the source region were extracted from the CEP data synopsis of 6/18/75 (Cherry, et al., 1975b).

2. The velocity-depth profile for the region above the working point was deduced from the same source. We also obtained a log to a depth of 2.3 km of the nearby hole UE19d from Dick Ramspot of LLL. This was used to construct a profile to that depth. The remainder of the crustal model for the body wave calculations is based on an average basin and range crust of Hill and Pakiser (1967).

3. Since we had little or no information about crustal structure at each of the receiver locations specified by the Project Officer, the same average crustal model was used at all stations for the body wave calculations.

4. For the initial prediction of body waves, two upper mantle models were used. These are HWNE from Helmberger and Wiggins (1971) and an unpublished model by Anderson, Hart and Jordan called C2AJ. Detailed studies of data recorded at stations on a northerly azimuth and 30-36° from NTS found C2AJ, slightly modified, to be the preferred model. At the time of the first prediction we had not accumulated enough experience at other azimuths and distances to make a reliable selection of an appropriate model.

5. For the initial prediction of surface waves the earth model CIT109 (Archambeau, Flinn and Lambert (1969)) was used, mainly because it was computationally convenient. However, this model was primarily based on inversion of body wave data and the crustal layers were meant to be generally applicable to shield areas.

6. For the revised predictions of body waves, all features of the calculation were held the same except different earth upper mantle models were used. The new models were a modified version of HWNE and a modified version of HWA (Wiggins and Helmberger (1973)). The modifications were primarily motivated by a study of the Mast observations.

7. We are currently evaluating a number of crustal models for an improved prediction of surface waves.

8. The instrument transfer functions were those provided by the Project Officer.

Incidental to the predictions, we have been evaluating the quality (for short period observations) of the SDCS stations at which the predictions are being made. The station quality is quantized in terms of (1) the amount of energy converted to tangential ground motion; (2) the coda length which is representative of internal reflection and scattering at the receiver, and (3) the amplitude coupling of the station. The latter is a quantization of that portion of the amplitude response of a station which is independent of azimuth and distance.

The first conclusion from our station quality estimate is that the FNWV site is of low quality and its usefulness (for short period observations) to the SDCS network should be reevaluated. We need to obtain more data to firmly evaluate the other stations but are in the process of doing so.

The comparison between our theoretical and the observed seismograms will now be presented. In Figs. 3.1 and 3.2 the initial short period predictions are shown together with the observations. Computed seismograms for the two upper mantle models C2AJ and HWNE are shown. From both the theoretical and observed records two amplitudes were measured. The first is the "b" amplitude which is the peak-to-peak amplitude of the first cycle on the record, corrected for the instrument response at the apparent period (i.e., twice the time separation between the measured peaks). The second is denoted the "d" phase. The nomenclature arises from the convention for measuring m_b followed for the LRSM network wherein the maximum cycle in the first few cycles on the wave train is measured. The cycle used for this amplitude is indicated on each seismogram.

The comparison between theoretical and observed "b" and "d" phases from Figs. 3.1 and 3.2 are shown in Figs. 3.3 and 3.4. Examining the wave form comparison in Figs. 3.1 and 3.2 we conclude that many of the important features of the

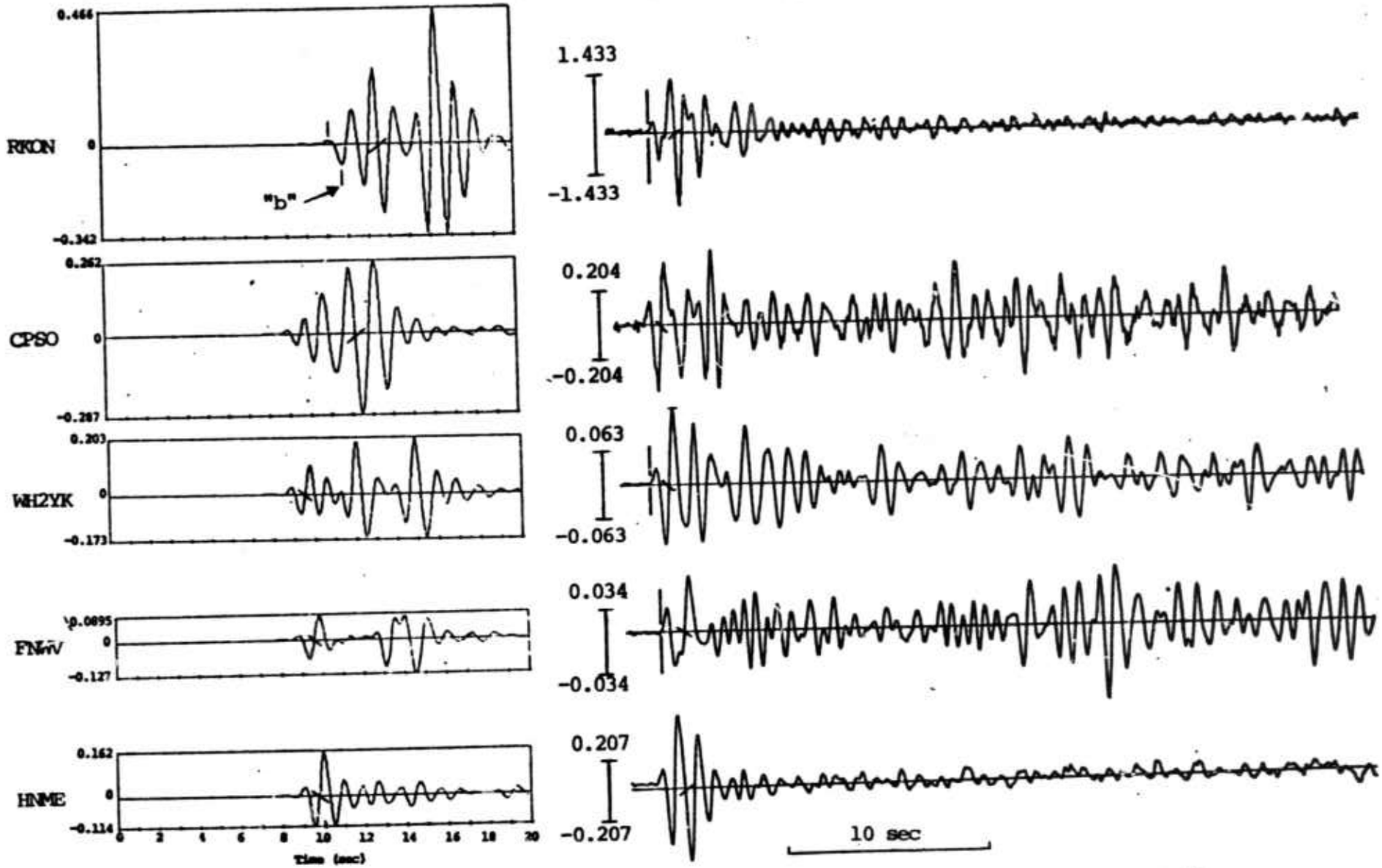

Figure 3.1. Comparison of theoretical (left) and observed seismograms for Mast at five SDCS stations. The upper mantle model for the theoretical calculations is C2AJ. The amplitude scale is indicated in microns at one second.

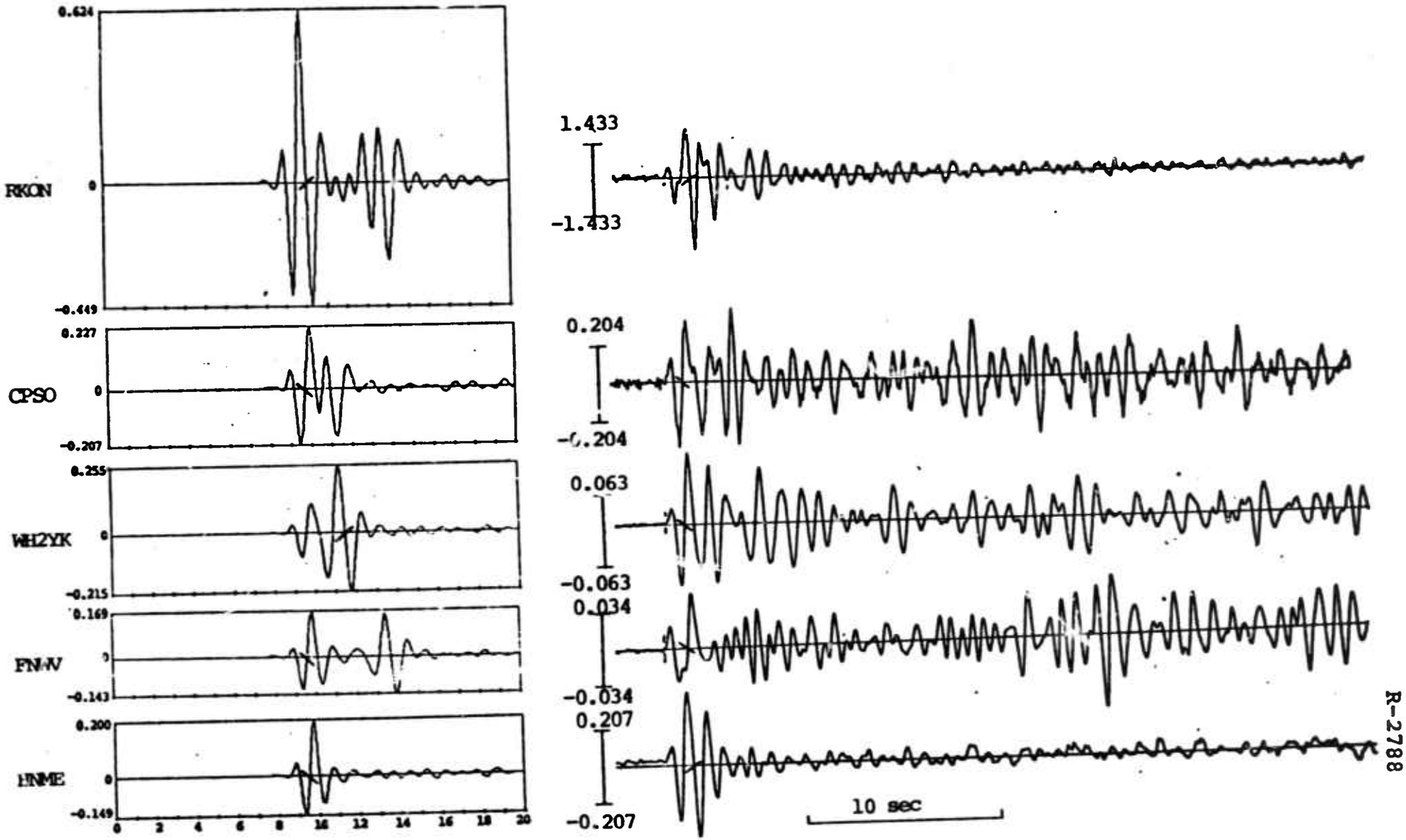

Figure 3.2. Comparison of theoretical and observed seismograms as in Fig. 3.1 except that the upper mantle model HWNE was used.

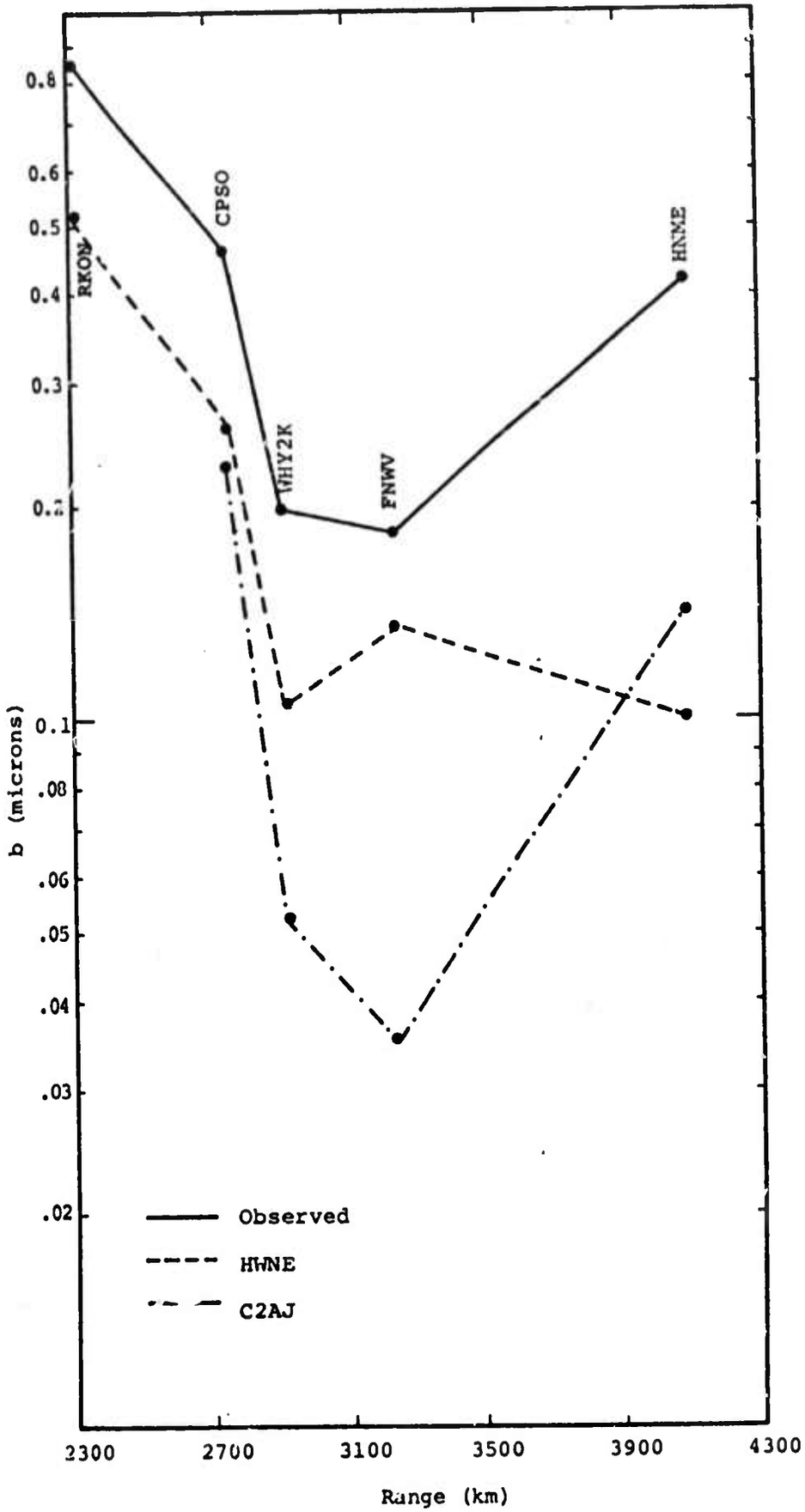

Figure 3.3. Comparison of observed and theoretical "b" amplitudes from Figs. 3.1 and 3.2.

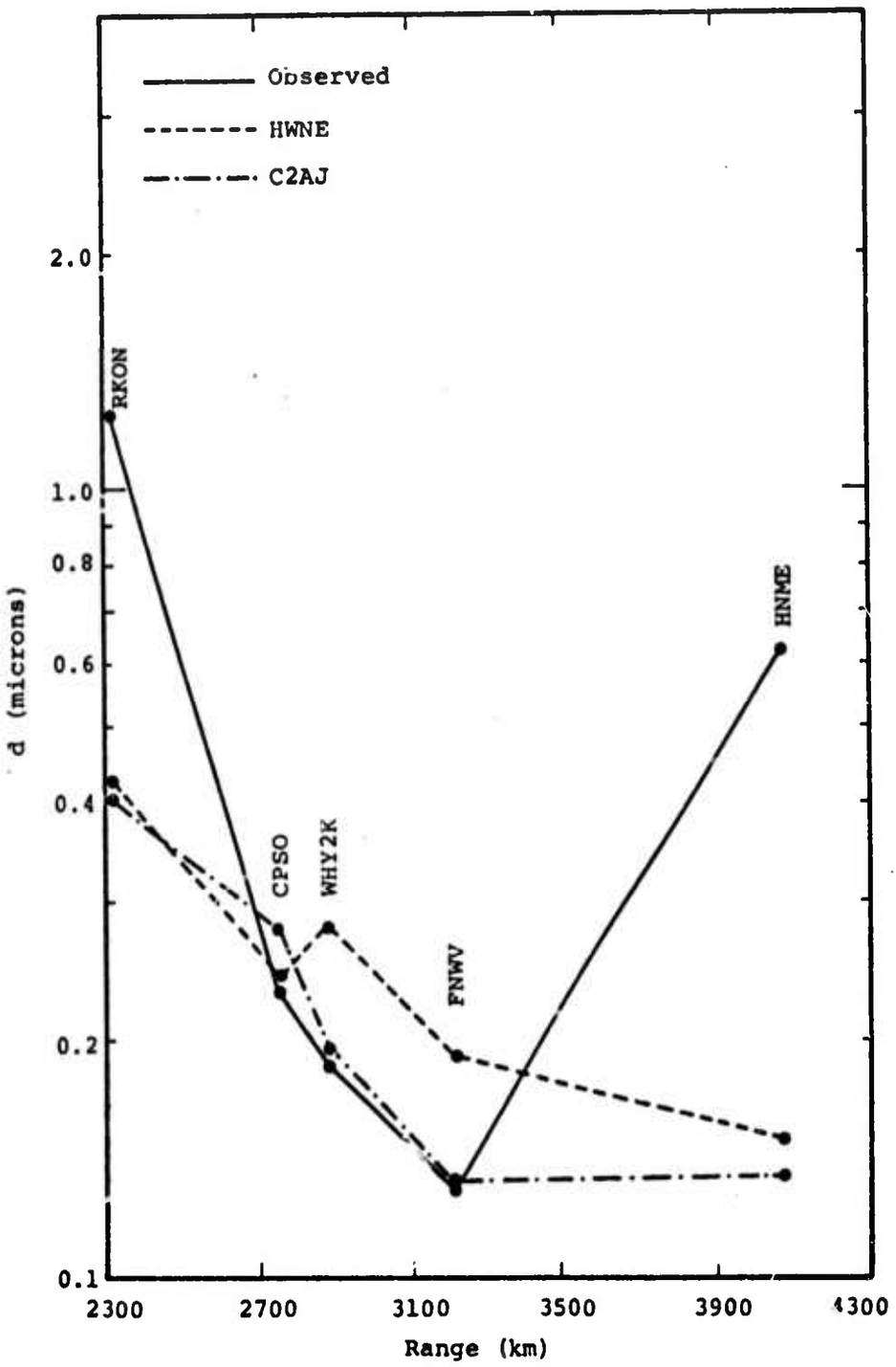

Figure 3.4. Comparison of observed and theoretical d amplitudes from Figs. 3.1 and 3.2.

seismogram are predicted by the model but that the comparison is far from ideal. The theoretical b amplitudes are substantially smaller than the observed. Our models should be most accurate in predicting this portion of the wave train. The agreement between d amplitudes, the phase from which conventional m_b is determined, is somewhat better. However, this is to some extent fortuitous since all the interfering phases which contribute to the d amplitude do not appear to be properly included in our calculations.

An effort was made to select an improved upper mantle model to give closer agreement between theory and observations. Implicit in this exercise is the assumption that the source and its vicinity is correctly modeled. A separate study (Bache, et al., 1975c) shows that such confidence is warranted.

The results of the more recent theoretical seismogram calculations are shown in Figs. 3.5 and 3.6 for two earth models: HWA-2 and HWNE-3. The amplitude comparisons for the "b" and "d" amplitudes are shown in Figs. 3.7 and 3.8. In our study of station characteristics, the FNWV station was found to give amplitudes that are three times smaller than expected, irrespective of epicentral distance. Therefore, the observed amplitudes for FNWV plotted in Figs. 3.7 and 3.8 have been multiplied by the station correction factor of three.

The waveform comparisons for the new predictions, Figs. 3.4 and 3.5, are perhaps a bit better than for the initial predictions, Figs. 3.1 and 3.2. Our model still does not successfully account for all the early arriving, interfering phases that control the shape of the first few seconds of the RKON and CPSO records. However, it does appear that the factors controlling the amplitude of the b phase are properly included in the model. Evaluation of the

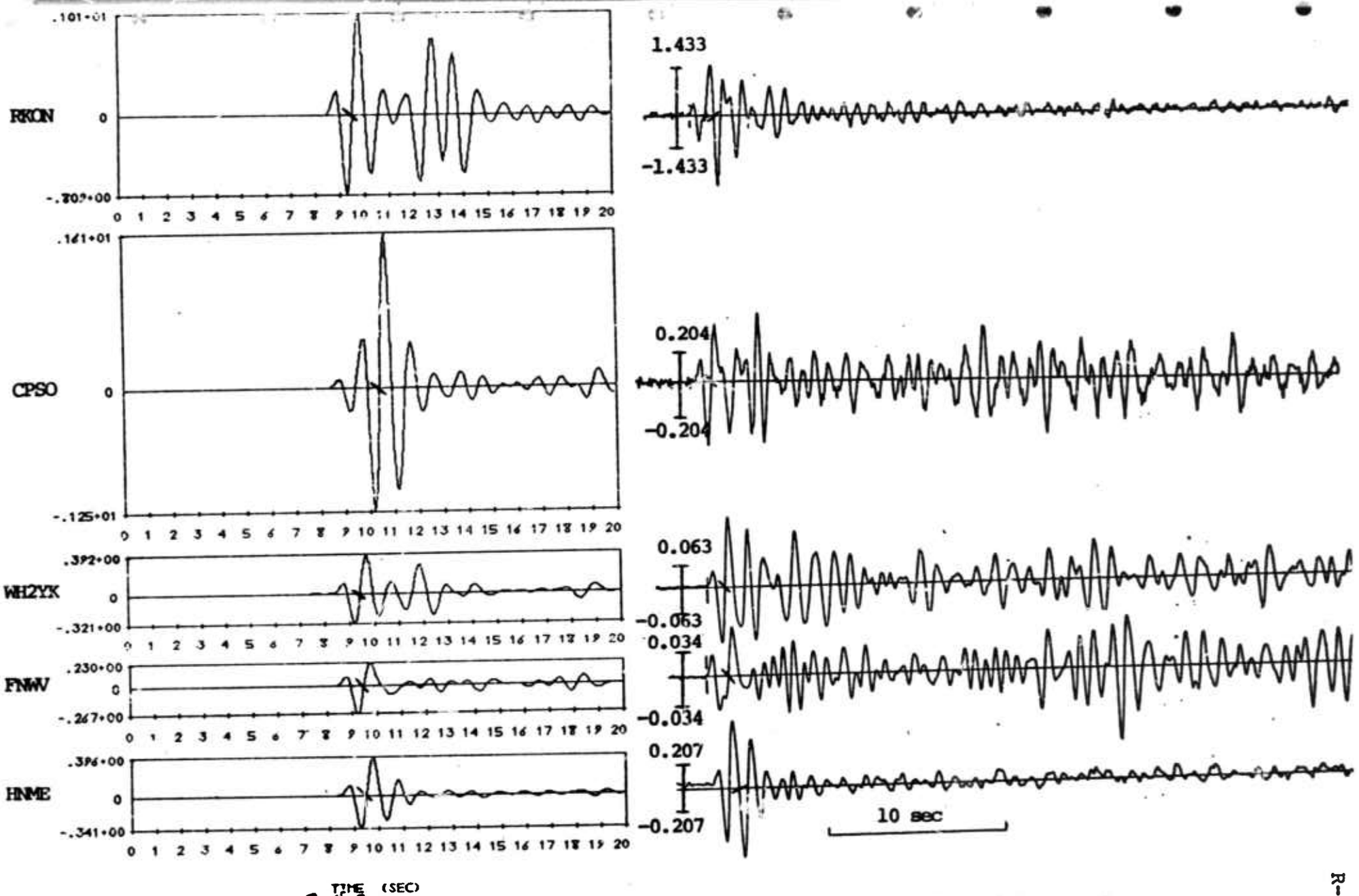

Figure 3.5. Short period vertical seismograms: observations on the right, and synthetics for the model HWA-2 on the left. The amplitude scale is indicated in microns at one second.

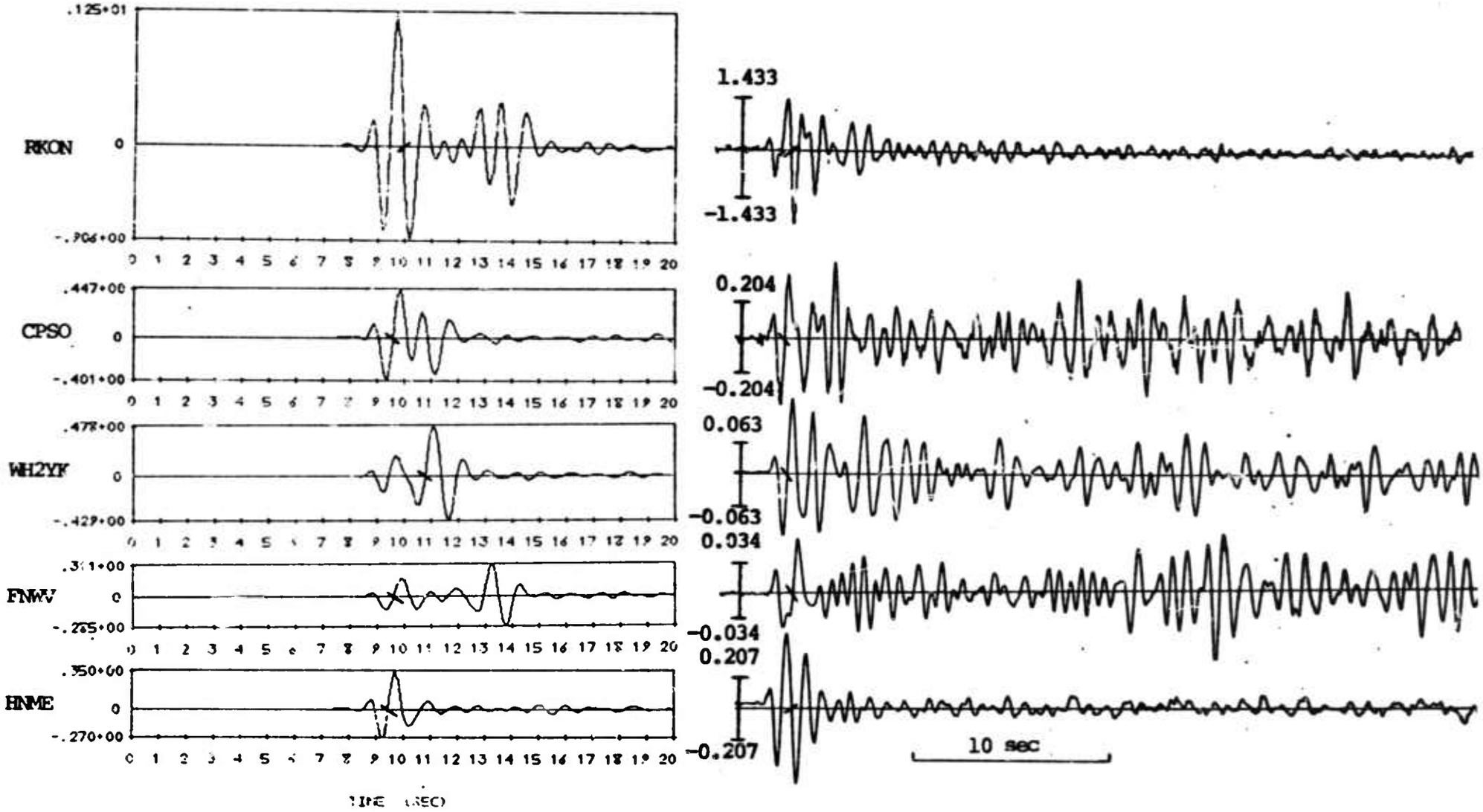

Figure 3.6. Short period vertical seismograms: observations on the right and synthetics for model HWNE-3 on the left.

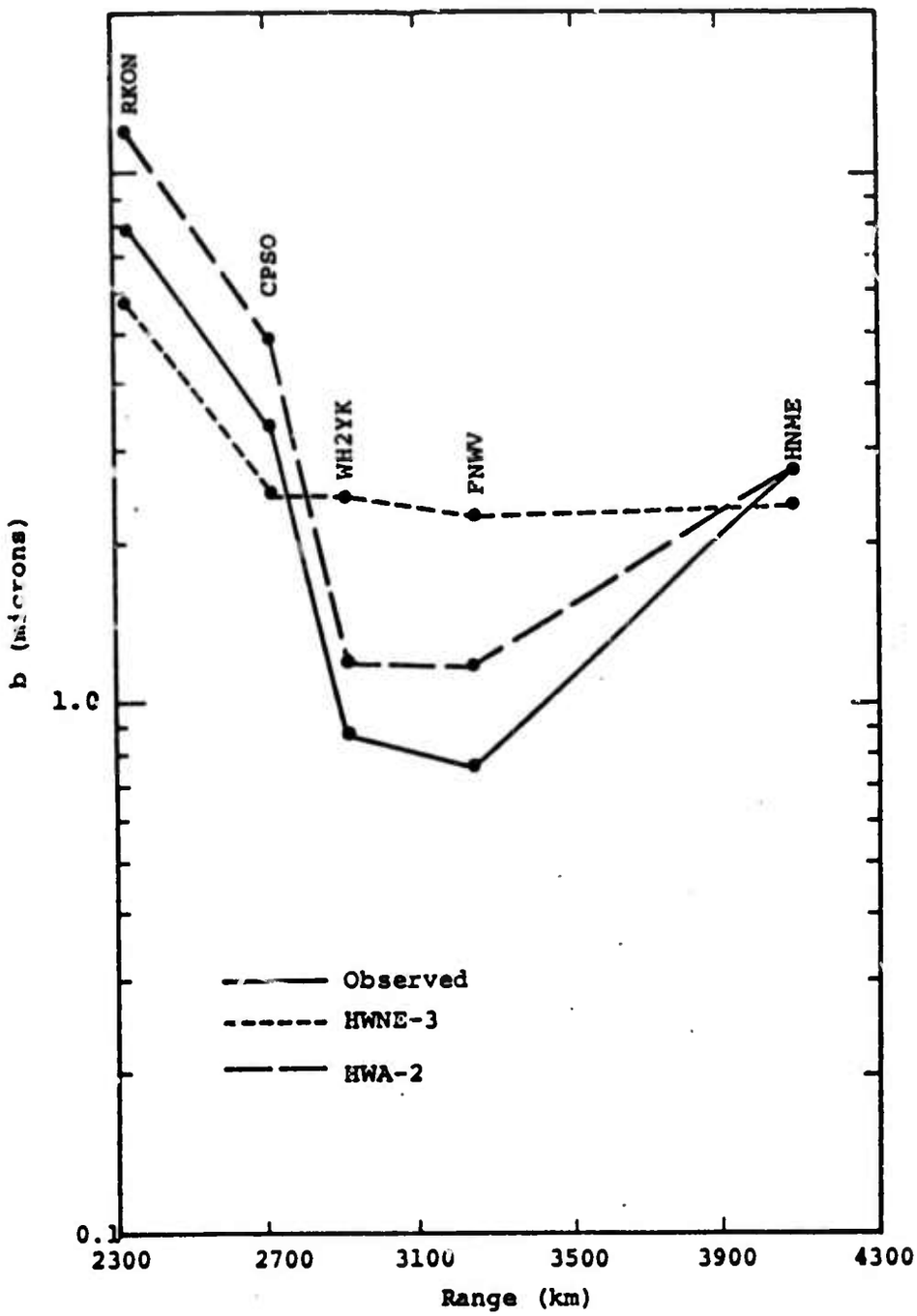

Figure 3.7. Comparison of observed and theoretical b amplitudes from the records of Figs. 3.5 and 3.6.

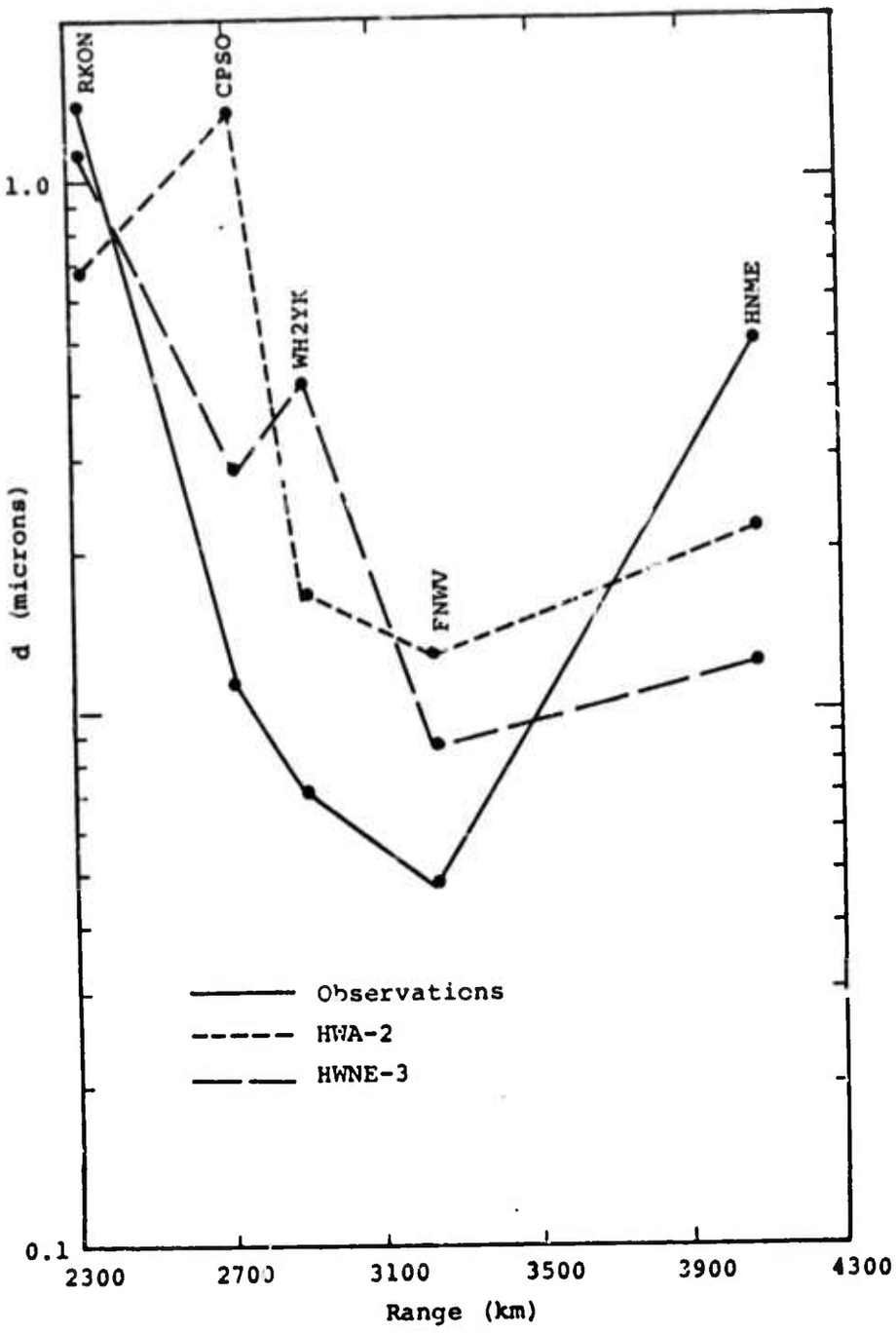

Figure 3.8. Comparison of predicted and observed d amplitudes from the records of Figs. 3.5 and 3.6.

predictions should rely most heavily on the b phase comparison since this phase is least affected by phenomena not related to the explosion coupling into elastic waves.

For the b amplitude the comparison (Fig. 3.6) between predicted and observed data is quite favorable, particularly for the HNME-3 model. At several stations the two models span the observations. Taking HNME-3 alone, the amplitudes are consistently within 30-50 percent of the observations.

For the d amplitude, the measurements are much more scattered, as might be expected.

3.1.2 Rayleigh Waves

The comparison between predicted and observed Rayleigh surface waves for the propagation path model CIT109 is shown in Figs. 3.9 and 3.10. The amplitude measurements in Fig. 3.10 are Airy phase measurements made on the indicated cycle on the long period vertical (LPZ) seismograms. The amplitudes are corrected for instrument response at the apparent period of the measured cycle.

As is immediately apparent from the observed and predicted travel times, the model CIT109 is not very appropriate for these stations. Since the predicted travel times are much lower than the observed, the crustal velocities in the model must be too high. As far as the amplitude comparison in Fig. 3.10 is concerned, the predicted Airy phase amplitude agrees quite well with the observed at RKON, a station on the Canadian shield for which the model CIT109 is perhaps most appropriate. At other stations, however, the predicted amplitudes are too low by an average factor of ≈2. We are currently constructing more appropriate propagation path models and will construct revised theoretical records which should exhibit much better agreement with the data.

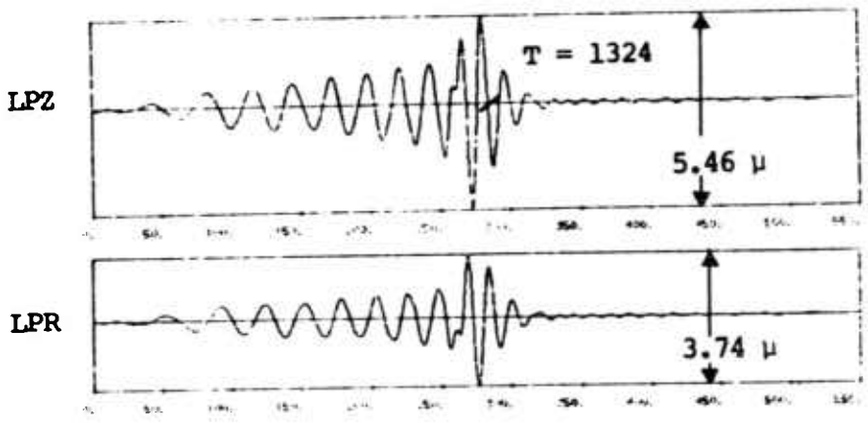

Figure 3.9. The theoretical long period record for HNME and the comparison of theoretical and observed long period data at RKON, CPSO, WHY2K and FNWV. The travel times, T, from detonation to the indicated zero crossing are given for all LPZ seismograms. The gain at 25 seconds period is indicated on each record. Both the vertical (LPZ) and radial (LPR) recordings are shown.

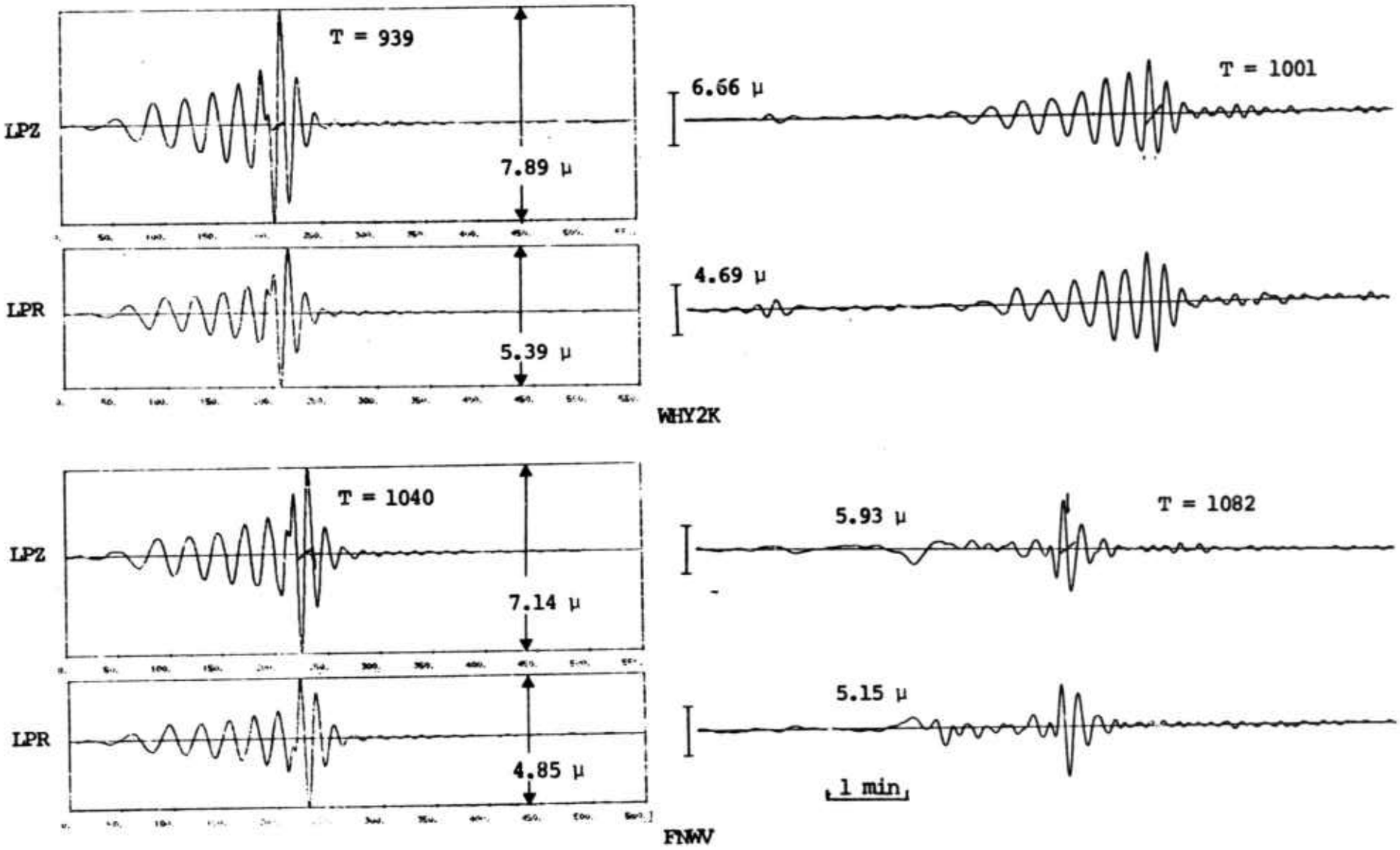
T = 939
LPZ
7.89 μ
LPR
5.39 μ
6.66 μ
T = 1001
4.69 μ
WHY2K
T = 1040
LPZ
7.14 μ
LPR
4.85 μ
5.93 μ
T = 1082
5.15 μ
1 min
FNW

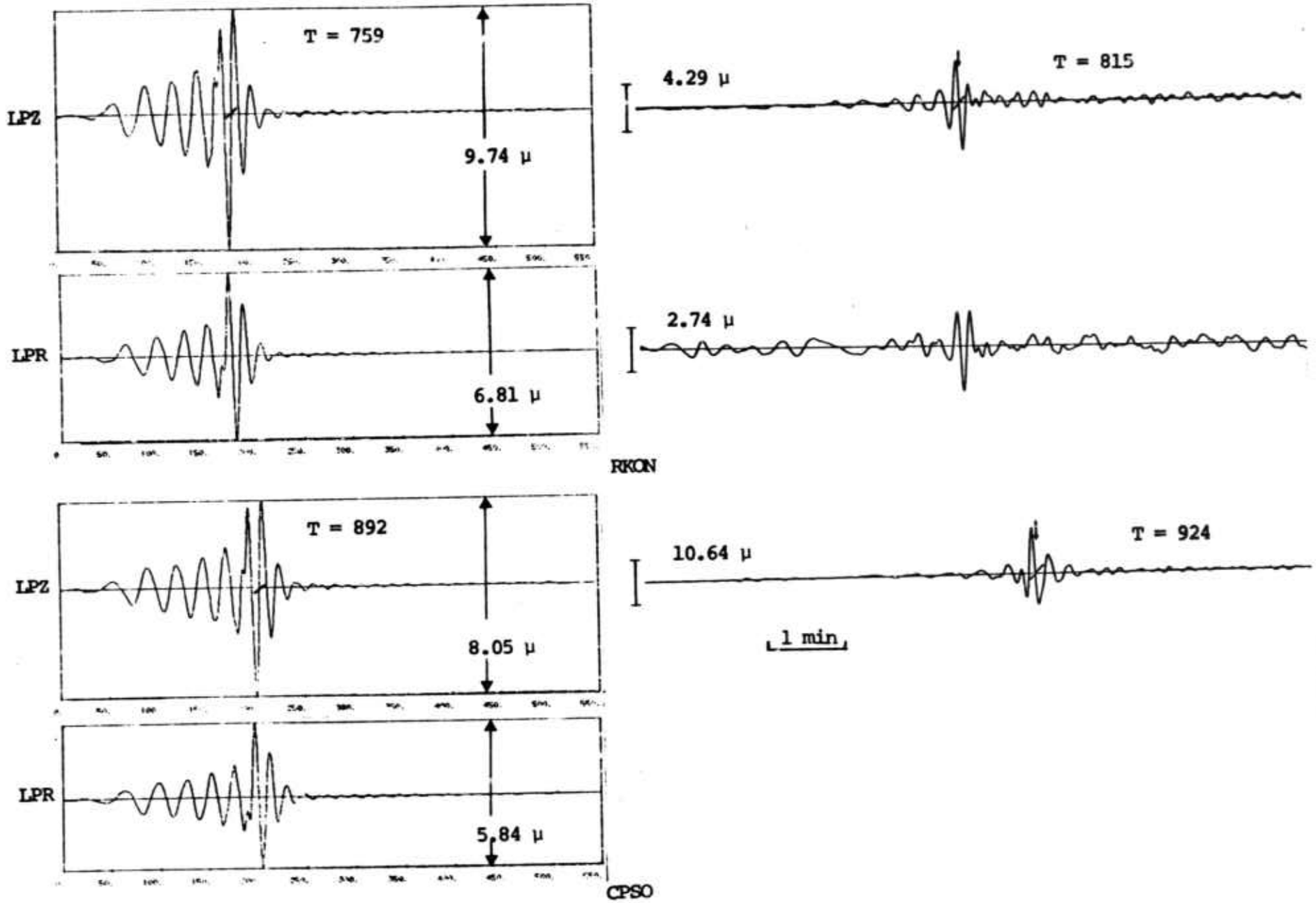
T = 759
LPZ
9.74 μ
LPR
6.81 μ
RKON
4.29 μ
T = 815
2.74 μ
T = 892
LPZ
8.05 μ
LPR
5.84 μ
CPSO
10.64 μ
T = 924
1 min

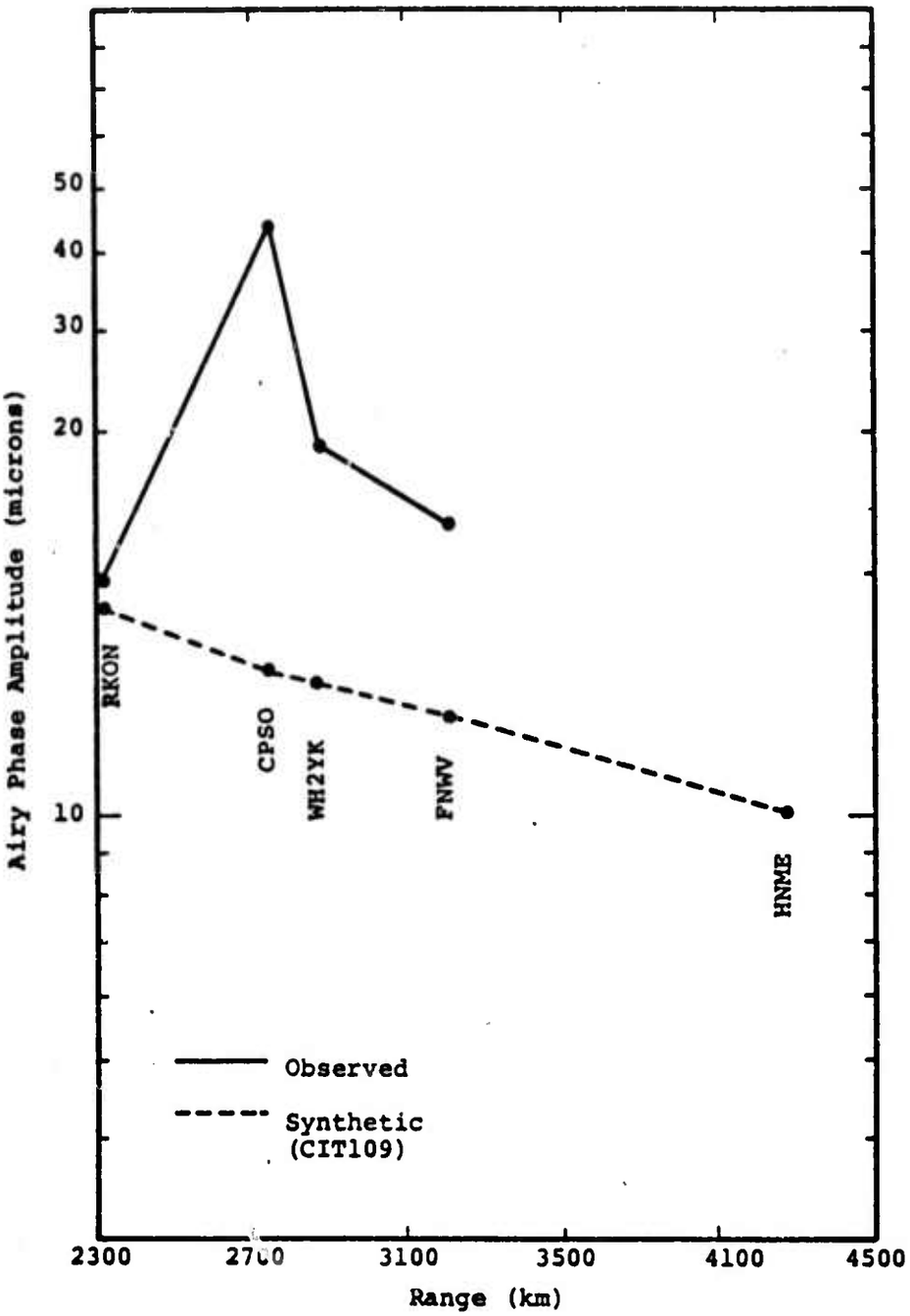

Figure 3.10. Comparison of predicted and observed Airy phase amplitudes from the records of Fig. 3.9.

3.2 MULTIPLE BURST CALCULATION

3.2.1 Introduction

Tension failure models employed in the CRAM code have provided insufficient information for many applications because crack strains were calculated entirely on the basis of the current magnitude and orientation of the principle coordinates. The crack direction was allowed to rotate with the principle coordinate system and therefore no meaningful information about crack orientation was provided. A new tension failure model which allows for the adjustment of crack strain components in a system of "failure coordinates" while holding the principle direction invariant is described in this section. This new model has been tested in a CRAM calculation involving simultaneous detonation of three closely spaced underground explosions and a graphical display is used to vividly depict the effect of shock interaction on crack orientation.

3.2.2 Discussion of the Tension Failure Model

An element is assumed to fail in tension if a principle stress is greater than zero and if the element has at any time experienced shear failure. We then apply the tension failure model proposed by Maenchen and Sack (1964) and introduce an inelastic strain normal to the crack. This inelastic strain is just sufficient to zero the principle tensile stress. The magnitude of the crack strains may be adjusted at later times to account for changes in the stress field, but the initial orientation of the crack is changed only to account for actual rotation of the element.

For example, in a cell which has experienced shear failure but remains uncracked, if $\hat{\sigma}_{11}$, $\hat{\sigma}_{22}$ and $\hat{\sigma}_{33}$ are the three principle stresses and if $\hat{\sigma}_{11}$ is greater than zero,

then the adjusted stresses (σ_{11}, σ_{22}, σ_{33}) are given by

$$\begin{aligned}
\sigma_{11} &= \hat{\sigma}_{11} - \left(k + \frac{4}{3}\mu\right) \Delta e_{11} \quad , \\
\sigma_{22} &= \hat{\sigma}_{22} - \left(k - \frac{2}{3}\mu\right) \Delta e_{11} \quad , \\
\sigma_{33} &= \hat{\sigma}_{33} - \left(k - \frac{2}{3}\mu\right) \Delta e_{11} \quad ,
\end{aligned} \tag{3.1}$$

where

$$\Delta e_{11} = \frac{\hat{\sigma}_{11}}{k + \frac{4}{3}\mu} \quad , \tag{3.2}$$

k is the bulk modulus, μ is the shear modulus and all stresses include the overburden pressure.

If two of the principle stresses, say $\hat{\sigma}_{11}$ and $\hat{\sigma}_{22}$, are greater than zero, then the stress adjustment becomes

$$\begin{aligned}
\sigma_{11} &= \hat{\sigma}_{11} - \left(k - \frac{2}{3}\mu\right) (\Delta e_{11} + \Delta e_{22}) - 2\mu\, \Delta e_{11} \quad , \\
\sigma_{22} &= \hat{\sigma}_{22} - \left(k - \frac{2}{3}\mu\right) (\Delta e_{11} + \Delta e_{22}) - 2\mu\, \Delta e_{22} \quad , \\
\sigma_{33} &= \hat{\sigma}_{33} - \left(k - \frac{2}{3}\mu\right) (\Delta e_{11} + \Delta e_{22}) \quad ,
\end{aligned} \tag{3.3}$$

where

$$\begin{aligned}
\Delta e_{11} &= \frac{\left(k + \frac{4}{3}\mu\right)\hat{\sigma}_{11} - \left(k - \frac{2}{3}\right)\mu\, \hat{\sigma}_{22}}{4\mu\left(k + \frac{\mu}{3}\right)} \quad , \\
\Delta e_{22} &= \frac{\left(k + \frac{4}{3}\mu\right)\hat{\sigma}_{22} - \left(k - \frac{2}{3}\mu\right)\hat{\sigma}_{11}}{4\mu\left(k + \frac{\mu}{3}\right)} \quad .
\end{aligned} \tag{3.4}$$

The above procedure is followed only for the initial formation of the crack. The orientation of the principle coordinates on the cycle during which a crack forms is defined by the angle α (see Fig. 3.11) which is adjusted only for actual rotation of the element during the remainder of a calculation. The coordinates located by the angle α are defined as the "failure coordinates" (1′, 2′, 3′). All subsequent adjustments to the crack strains are performed in the failure coordinate system. The tensile crack strains are adjusted such that all tensions which appear in the element are eliminated. Additionally, a shear component of the crack strain tensor is introduced and adjusted such that the orientation of the principle coordinates, (1, 2, 3), remains constant. The relative orientation of the (X, Y), (2, 3) and (2′, 3′) coordinates is illustrated in Fig. 3.12. Note that the principle coordinates are located by the angle ϕ and that $\theta = \alpha - \phi$ is the angle between the principle coordinates and the crack coordinates.

For example, in a cell which has already failed in tension, if $\hat{\sigma}_{1'1'}$, $\hat{\sigma}_{2'2'}$, $\hat{\sigma}_{3'3'}$ and $\hat{\tau}_{2'3'}$ are the failure stresses and if $\hat{\sigma}_{1'1'}$ is greater than zero, then the adjusted stresses ($\sigma_{1'1'}$, $\sigma_{2'2'}$, $\sigma_{3'3'}$, $\tau_{2'3'}$) are given by

$$\begin{aligned}
\sigma_{1'1'} &= \hat{\sigma}_{1'1'} - \left(k + \frac{4}{3}\mu\right) \Delta e_{1'1'} \,, \\
\sigma_{2'2'} &= \hat{\sigma}_{2'2'} - \left(k - \frac{2}{3}\mu\right) \Delta e_{1'1'} \,, \\
\sigma_{3'3'} &= \hat{\sigma}_{3'3'} - \left(k - \frac{2}{3}\mu\right) \Delta e_{1'1'} \,, \\
\tau_{2'3'} &= \hat{\tau}_{2'3'} - 2\mu \, \Delta e_{2'3'} \,,
\end{aligned} \tag{3.5}$$

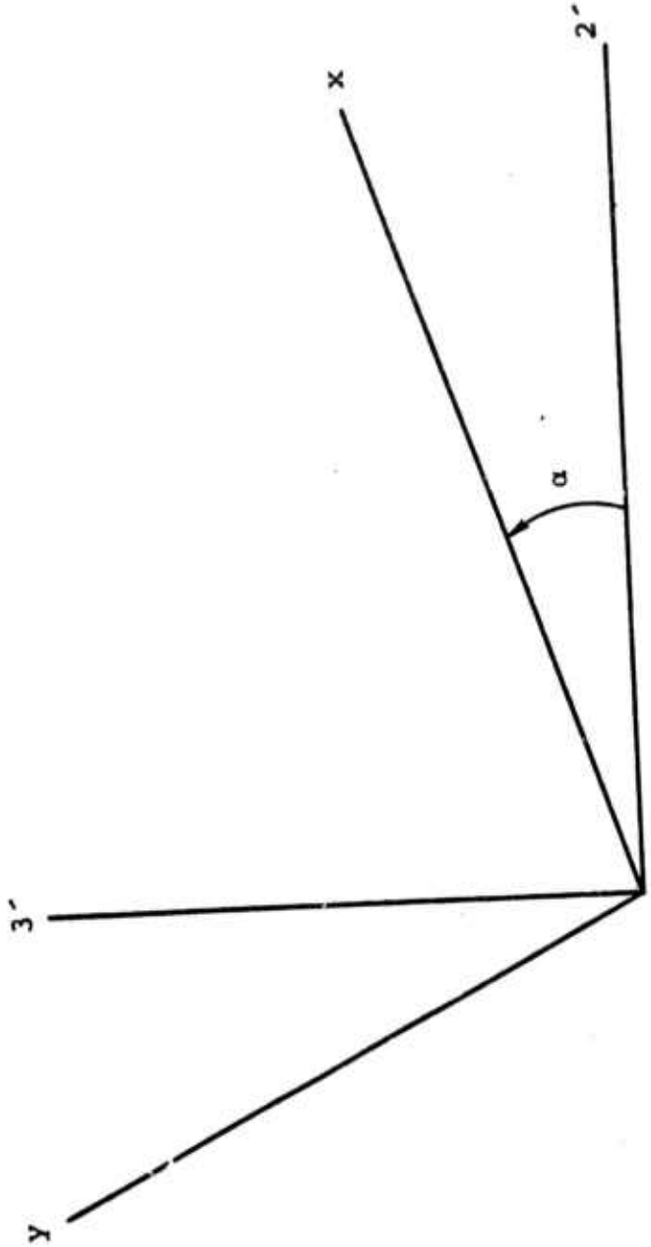

Figure 3.11. Schematic definition of the crack angle α and the failure coordinates.

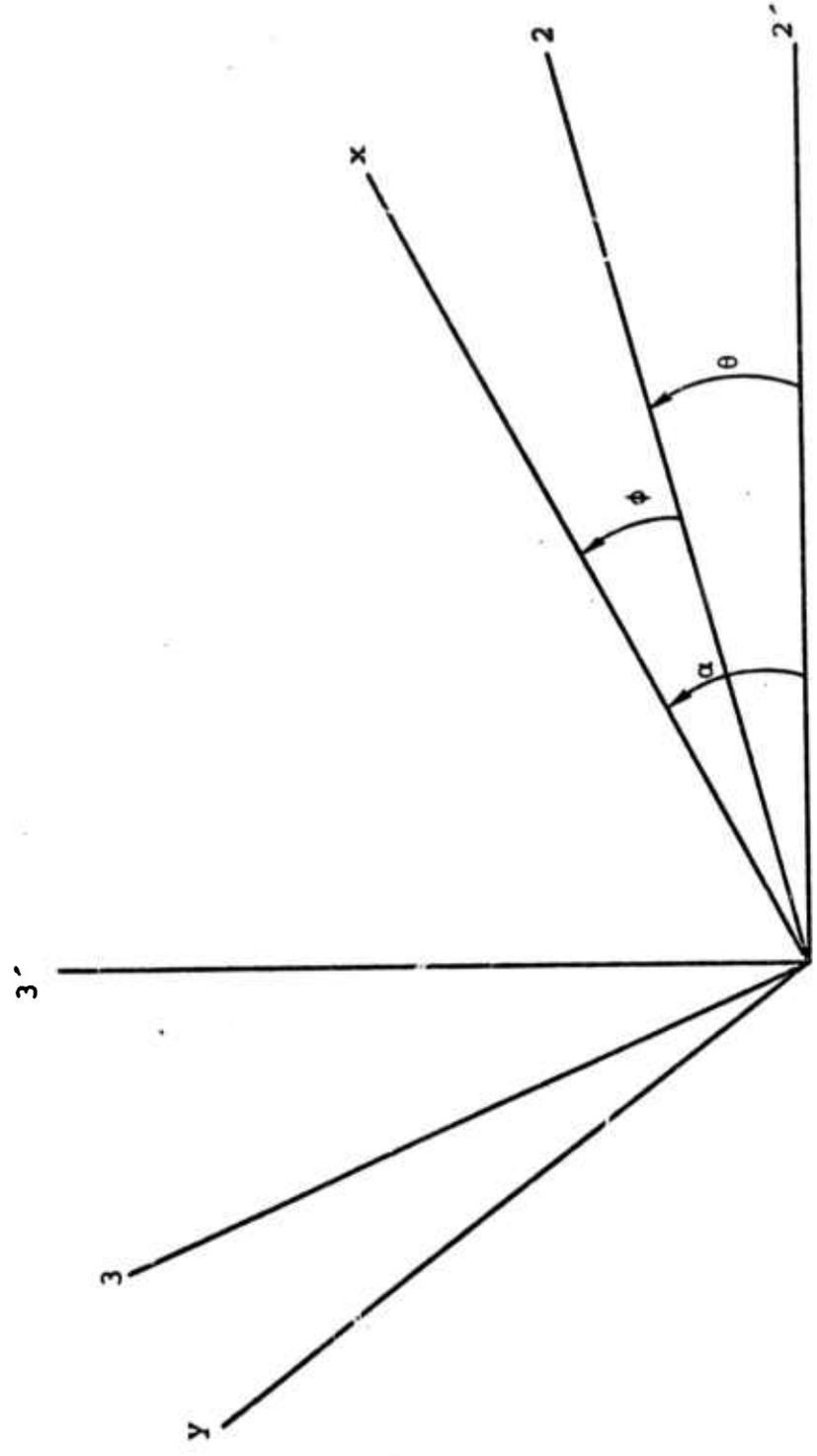

Figure 3.12. Relative orientation of the principal and failure coordinate systems.

where

$$\Delta e_{1'1'} = \frac{\hat{\sigma}_{1'1'}}{k + \frac{4}{3}\mu} \quad , \tag{3.6}$$

$$\Delta e_{2'3'} = \frac{\Delta e_{2'2'} - \Delta e_{3'3'}}{2} \tan 2\theta = 0 \quad .$$

If the failure stresses $\hat{\sigma}_{1'1'}$ and $\hat{\sigma}_{2'2'}$ are both greater than zero then the stress adjustment becomes

$$\begin{aligned}
\sigma_{1'1'} &= \hat{\sigma}_{1'1'} - \left(k - \tfrac{2}{3}\mu\right)(\Delta e_{1'1'} + \Delta e_{2'2'}) - 2\mu\, \Delta e_{1'1'}, \\
\sigma_{2'2'} &= \hat{\sigma}_{2'2'} - \left(k - \tfrac{2}{3}\mu\right)(\Delta e_{1'1'} + \Delta e_{2'2'}) - 2\mu\, \Delta e_{2'2'}, \\
\sigma_{3'3'} &= \hat{\sigma}_{3'3'} - \left(k - \tfrac{2}{3}\mu\right)(\Delta e_{1'1'} + \Delta e_{2'2'}) \quad , \\
\tau_{2'3'} &= \hat{\tau}_{2'3'} - 2\mu\, \Delta e_{2'3'} \quad ,
\end{aligned} \tag{3.7}$$

where

$$\Delta e_{1'1'} = \frac{\left(k + \frac{4}{3}\mu\right)\hat{\sigma}_{1'1'} - \left(k - \frac{2}{3}\mu\right)\hat{\sigma}_{2'2'}}{4\mu\left(k + \frac{\mu}{3}\right)} \quad ,$$

$$\Delta e_{2'2'} = \frac{\left(k + \frac{4}{3}\mu\right)\hat{\sigma}_{2'2'} - \left(k - \frac{2}{3}\mu\right)\hat{\sigma}_{1'1'}}{4\mu\left(k + \frac{\mu}{3}\right)} \quad , \tag{3.8}$$

$$\Delta e_{2'3'} = \frac{\Delta e_{2'2'} - \Delta e_{3'3'}}{2} \tan 2\theta = \frac{\Delta e_{2'2'}}{2} \tan 2\theta \quad .$$

All the normal inelastic strain increments ($\Delta e_{1'1'}$, $\Delta e_{2'2'}$, $\Delta e_{3'3'}$) are accumulated on each cycle giving

$$E^{n+1}_{1'1'} = E^{n}_{1'1'} + \Delta e_{1'1'} \ ,$$

$$E^{n+1}_{2'2'} = E^{n}_{2'2'} + \Delta e_{2'2'} \ , \qquad (3.9)$$

$$E^{n+1}_{3'3'} = E^{n}_{3'3'} + \Delta e_{3'3'} \ .$$

These equations apply equally well for crack closure. If at least one of the total strains in Eq. (3.9) is greater than zero (say $E^{n}_{1'1'}$), then the crack will open or close depending on the sign of $\hat{\sigma}_{11}$. If $\hat{\sigma}_{11} > 0$ then

$$\Delta e_{11} > 0 \ ,$$

$$E^{n+1}_{1'1'} > E^{n}_{1'1'} \ ,$$

and the crack width increases. The inequalities are reversed if $\hat{\sigma}_{1'1'} < 0$ and the crack width decreases. Closure will continue until

$$E^{n}_{1'1'} + \Delta e_{1'1'} < 0 \ .$$

Then

$$\Delta e_{1'1'} = -E^{n}_{1'1'} \ ,$$

$$E^{n+1}_{1'1'} = 0 \ ,$$

and the crack is completely closed. When this state is achieved the element is then able to support a compressive stress in the (1′, 0, 0) direction.

3.2.3 Results of Multiple Burst Calculation

The new tension failure model has been incorporated into the CRAM code and used in the calculation of ground motion due to simultaneous detonation of three 15 kton explosive sources. The sources were spaced 165 meters apart on a horizontal axis. The calculation was initiated with the SKIPPER code in spherical symmetry and linked to the CRAM in axial symmetry by initializing the CRAM mesh just prior to shock interaction between adjacent sources.

Grid plots showing the formation of cracks as shock interaction occurs are presented at successive times in Figs. 3.13, 3.14, 3.15 and 3.16. The right boundary in these figures is a plane of symmetry and the lower boundary is an axis of symmetry. Elements which have developed cracks are marked with dots and/or lines. The dots represent cracks which lie in planes passing through the axis of symmetry. The lines represent cracks which lie in planes which are perpendicular to the figure and pass through the given line; thus the lines provide a convenient display of the crack orientation. Note that in Fig. 3.13 hoop cracks due to radial expansion of the cavities are beginning to form. In Fig. 3.14 shock interaction has caused adjacent sources to be connected by a series of hoop cracks. Extensive cracking appears above and between the adjacent sources in Fig. 3.15; this cracking is in the plane of the grid plot and indicates that the two spherical sources resemble a line source at moderate distances from the axis of symmetry. In Fig. 3.16 cracks have covered most of the grid.

3.2.4 Summary

A new tension failure model has been developed and incorporated into the CRAM code. The new model retains the orientation of the crack at initial failure. Subsequent

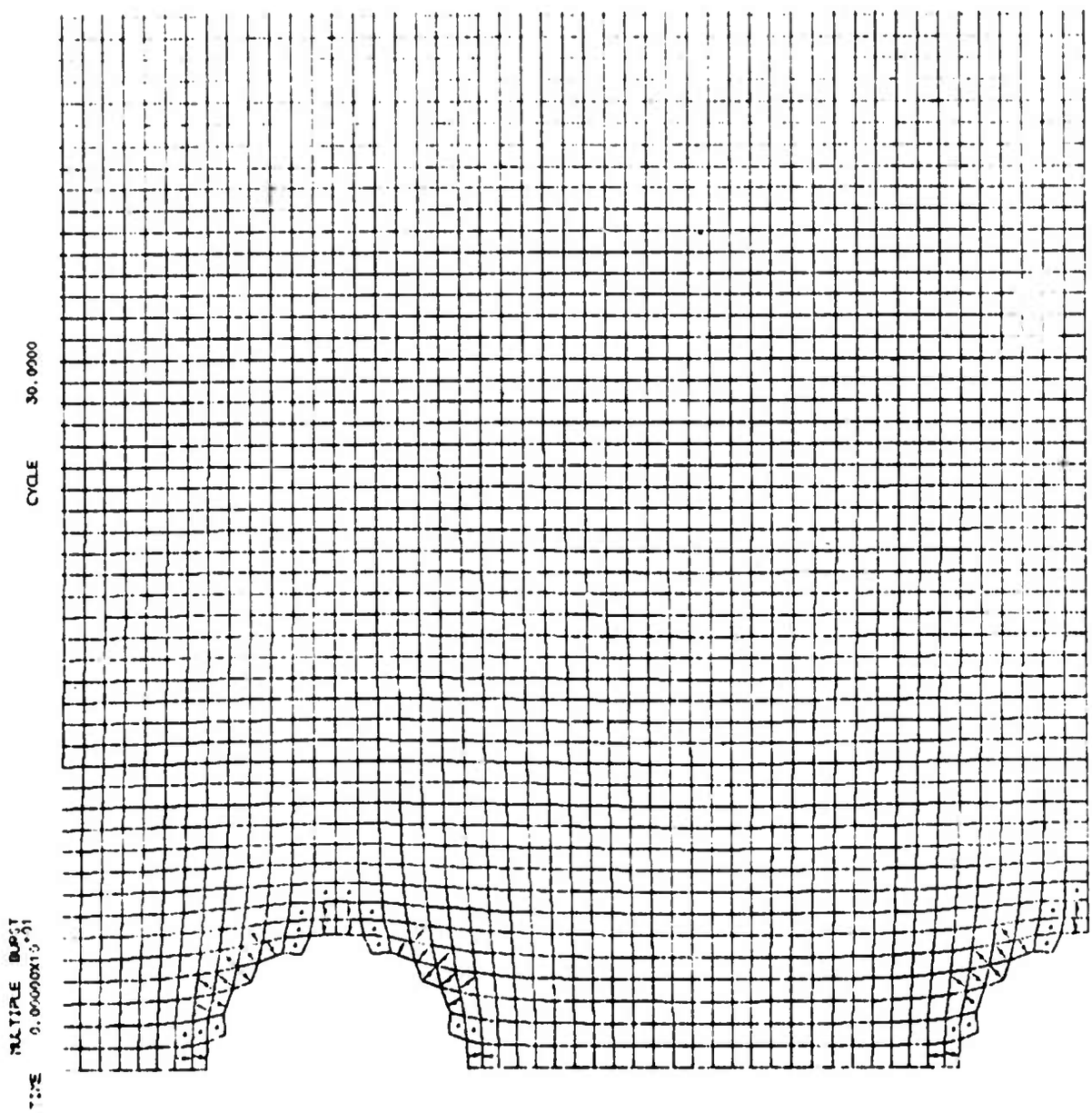

Figure 3.13. Crack location and orientation 4.93 msec after detonation.

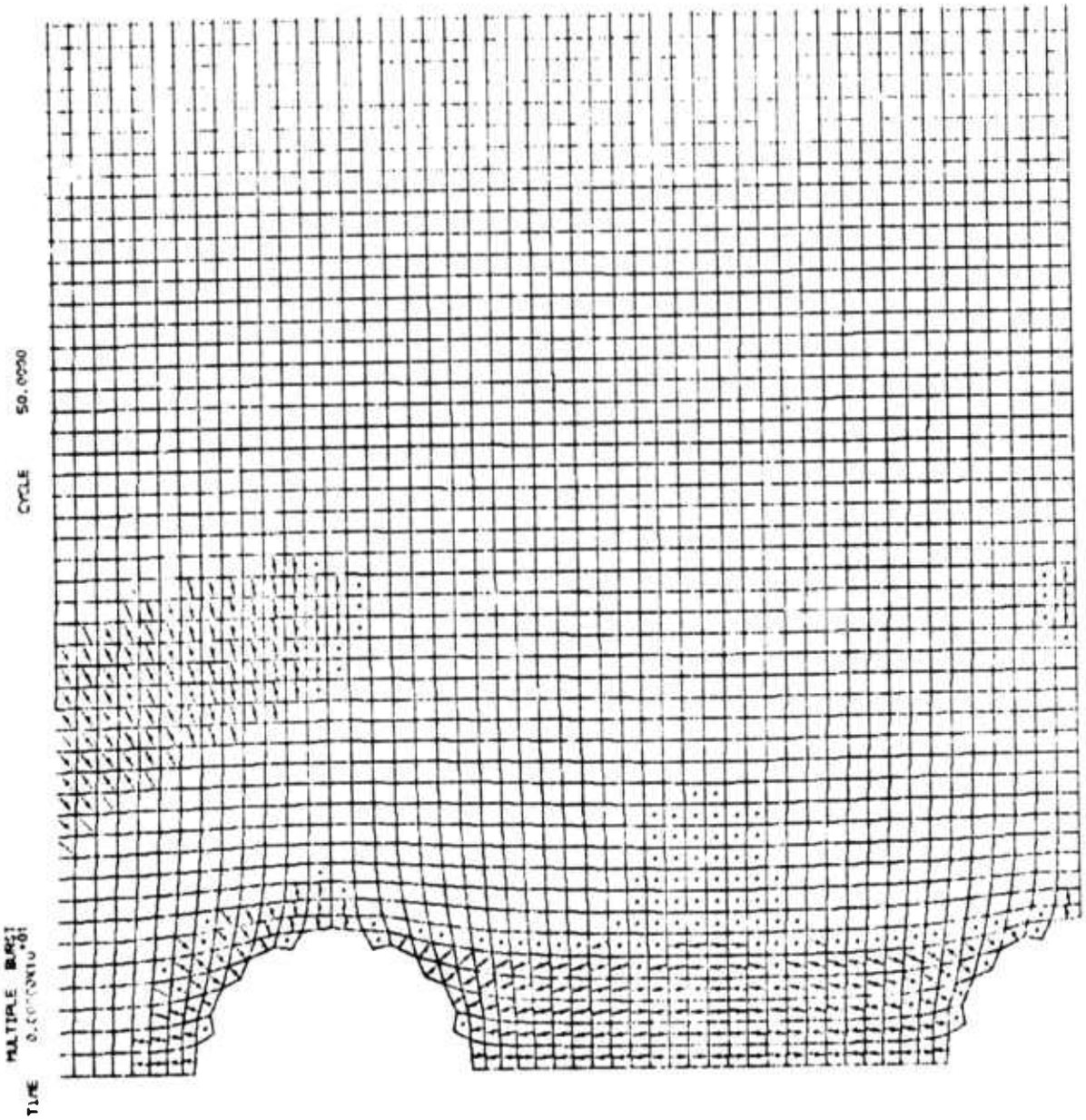

Figure 3.14. Crack location and orientation 6.85 msec after detonation.

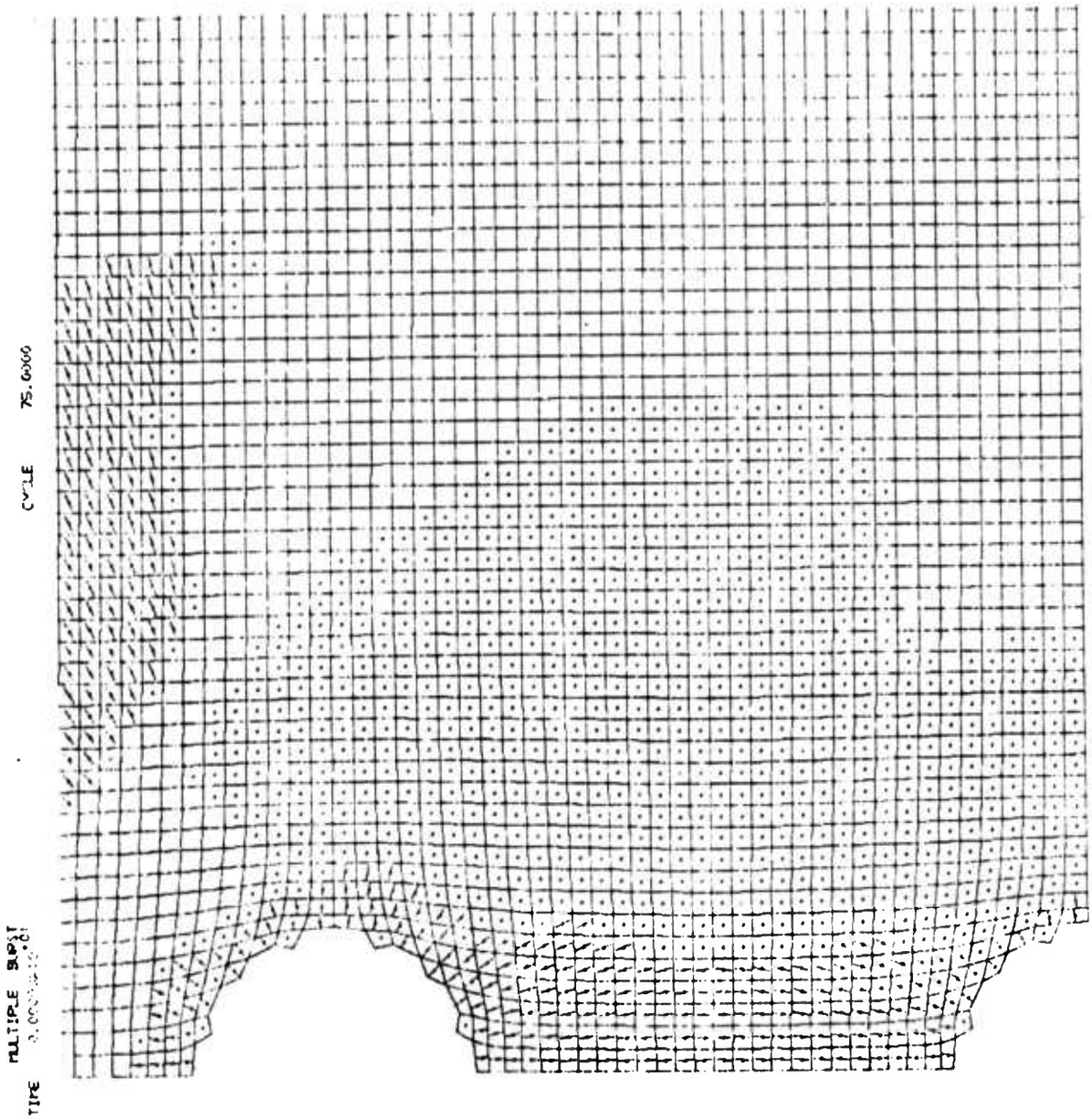

Figure 3.15. Crack location and orientation 9.21 msec after detonation.

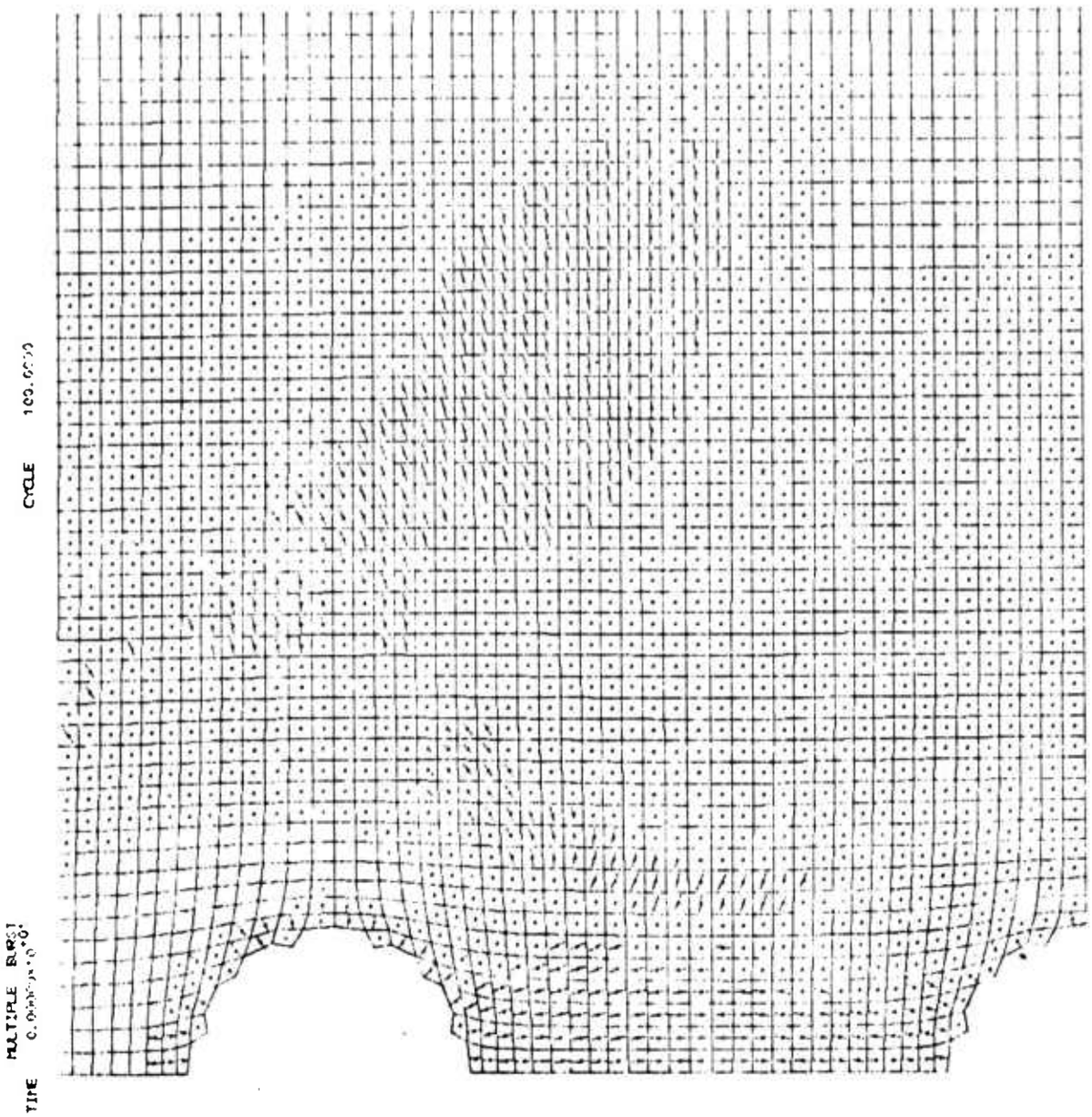

Figure 3.16. Crack location and orientation 11.5 msec after detonation.

adjustment of the crack strains is accomplished in a manner which holds the principle directions invariant thereby preserving stability.

3.3 SEISMIC COUPLING FROM A NUCLEAR EXPLOSION

3.3.1 Dependence of Seismic Coupling on the Near Explosion Source Environment

A special report that describes a parameter study of the dependence of seismic coupling on the nonlinear behavior of the near explosion source environment was submitted during this reporting period (Cherry, et al., 1975a). The results of this parameter study provide valuable insight concerning the importance of various material parameters with respect to accurate prediction of seismic coupling. In this study it was shown that increasing the overburden pressure, or, equivalently, the depth of burial, decreases coupling efficiency substantially. Therefore, the DOB must be accurately known in order to make a reliable prediction of seismic magnitude. It is also desirable to know the properties of the material in the immediate vicinity of the device; if substantial spatial variation of the material properties occurs near the device or if the DOB is quite shallow it may be necessary to consider two-dimensional effects which were not treated in the parameter study. Accurate prediction of seismic magnitudes via one-dimensional spherically symmetric calculations is therefore understood to be dependent on the material uniformity about the device.

In this study a relationship between teleseismic magnitude, m_b, and $\Psi(\infty)$, the steady state value of the reduced displacement potential (RDP), was given as

$$m_b \sim \log [c\, \Psi(\infty)] \qquad (3.10)$$

where c is the near source compressional wave speed. Based on Eq. (3.10), if $\Psi_i(\infty)$ and $\Psi_k(\infty)$ are two values of $\Psi(\infty)$ corresponding to materials i and k then the changes in teleseismic magnitude is given by

$$\Delta m = m^i - m^k = \log \frac{c_i \Psi_i(\infty)}{c_k \Psi_k(\infty)} \tag{3.11}$$

Since the elastic properties of the near source material appear in the magnitude relation, Eq. (3.11), via the P wave velocity, c, it is obviously important to determine their values accurately. A positive error in determination of c would cause body wave magnitude to be over-predicted. A positive error in μ would cause magnitude to be under-predicted.

The steady state value of the RDP, $\Psi(\infty)$, which appears in the magnitude relation, Eq. (3.11), is dependent on the shock response of the near source material. The near source material properties which have the most pronounced effect on the shock response are the water mass fraction, f_w, and the air-filled void fraction, ϕ_0. Positive errors in either f_w or ϕ_0 could lead to substantial under-prediction of seismic magnitudes. Seismic magnitude is not very sensitive to P_e, the elastic pressure, and P_c, the crush pressure, indicating that details in the porosity model are relatively unimportant.

Seismic magnitudes are, however, very sensitive to the parameters which describe the failure surface. If Y_0, Y_m, or P_m are varied such that the material strength is enhanced the coupling efficiency of an explosive device is impaired. Thus, a positive error in the material strength would lead one to under-predict seismic magnitude.

3.3.2 Constitutive Modeling

A topical report by Garg (1975) was prepared and submitted during this contractual report period. This report deals with the development of constitutive relations for fluid-saturated porous media, suitable for inclusion in the CRAM or SKIPPER codes. The theoretical formulation is based on the models for fluid-saturated rock aggregates previously developed by Garg and Nur (1973). A method for including the new constitutive model in the standard hydrodynamic codes referred to above is also described in this report.

IV. CONCLUSIONS

Considerable progress was made during the second three-month period of this project on several of the tasks specified in the work statement of this contract.

Teleseismic ground motion predictions for the recent Pahute Mesa explosion, MAST, were quite successful in terms of both amplitude and waveform matching. The predicted short-period body wave amplitudes were within 30 to 50 percent of the observed amplitudes at most of the SDCS stations. In addition, the general character of the first few seconds of the P-wave trains at the various SDCS stations were matched in reasonable detail.

A tension failure model that describes the development of a region of enhanced tension failure (cracking) produced during stress release behind the interacting shock fronts from closely spaced explosions was developed. Calculations for a multiple explosion scenario (three closely spaced explosions detonated simultaneously) were carried out into the elastic region using the two-dimensional CRAM code with the new material failure model included.

V. REFERENCES

Archambeau, C. B., E. A. Flinn, and D. G. Lambert, "Fine Structure of the Upper Mantle," J. Geophys. Res., 74, 5825-5865, 1969.

Bache, T. C., T. G. Barker, J. T. Cherry, and J. M. Savino, "Prediction of Teleseismic Ground Motion from the Underground Explosion, MAST," Systems, Science and Software Report SSS-R-76-2727, September 1975a.

Bache, T. C., J. T. Cherry, K. G. Hamilton, J. F. Masso, and J. M. Savino, "Application of Advanced Methods for Identification and Detection of Nuclear Explosions from the Asian Continent," Systems, Science and Software Report SSS-R-75-2646, May 1975b.

Bache, T. C., J. T. Cherry, N. Rimer, J. M. Savino, T. R. Blake, T. G. Barker, and D. G. Lambert, "An Explanation of the Relative Amplitudes of the Teleseismic Body Waves Generated by Explosions in Different Test Areas at NTS," Systems, Science and Software Final Report for DNA, October 1975.

Cherry, J. T., N. Rimer, and W. O. Wray, "Seismic Coupling from a Nuclear Explosion: The Dependence of the Reduced Displacement Potential on the Nonlinear Behavior of the Near Source Rock Environment," Systems, Science and Software Report SSS-R-76-2742, September 1975a.

Cherry, J. T., N. Rimer, J. M. Savino, and W. O. Wray, "Improved Yield Determination and Event Identification Research," Systems, Science and Software Report SSS-R-75-2696, August 1975b.

Garg, S. K., "Constitutive Equations for Fluid-Saturated Porous Media," Systems, Science and Software Report SSS-R-76-2766, October 1975.

Garg, S. K., and A. Nur, "Effective Stress Laws for Fluid Saturated Porous Rocks," J. Geophys. Res., 78, 1973.

Harkrider, D. G., "Surface Waves in Multilayered Media. I. Rayleigh and Love Waves from Sources in a Multilayered Half-Space," Bull. Seism. Soc. Amer., 54, 627-679, 1964.

Harkrider, D. G., "Surface Waves in Multilayered Elastic Media. II. Higher Mode Spectra and Spectral Ratios from Point Sources in Plane Layered Earth Models," Bull. Seism. Soc. Amer., 60, 1937-1988, 1964.

Haskell, N. A., "Crustal Reflection of Plane P and SV Waves," J. Geophys. Res., 72, 2583-2587, 1962.

Helmberger, D. V., and R. A. Wiggins, "Upper Mantle Structure of the Midwestern United States," J. Geophys. Res., 76, 3229-3245, 1971.

Hill, P., and C. Pakiser, "Seismic-Refraction Study of Crustal Structure Between the Nevada Test Site and Boise, Idaho," Geol. Soc. of Amer. Bull., 78, 685-704, 1967.

Maenchen, G., and S. Sack, "The TENSOR Code," in Methods in Computational Physics, Vol. 3, Academic Press, New York, 1964.

Wiggins, R. A., and D. V. Helmberger, "Upper Mantle Structure of the Western United States," J. Geophys. Res., 78, 1870-1888, 1973.

Wiggins, R. A., and D. V. Helmberger, "Synthetic Seismogram Computation by Expansion in Generalized Rays," Geophys. J. R. Astr. Soc., 37, 73-90, 1974.